PC1

THE COHESIVE FORCE OF WATER

W. Widdas

Sutton St James, South Lincs, UK

In 1846 Faraday gave a lecture on the 'Cohesive Force of Water'. This property of water is still important. The Laplace formula for the pressure developed by the surface energy of liquid water in capillaries, $P = 2\gamma/r$, where γ is the surface energy (72×10^{-3} J m^{-2}) and r is the radius, is well known, and appears in physiological textbooks. The surface energy of water was an important part of the preclinical medical course seventy years ago, but has largely disappeared from the curriculum in the latter decades of the twentieth century. Biocomputation and molecular modelling were proposed eleven years ago as submicroscopic physiology (Widdas, 1993). Cellular biology and the properties of water, are reinvigorated by the application of the Laplace pressure to biological systems. Its use in muscular contraction was suggested by Bernstein in 1908, and Weizsacker (1914) when working with A.V. Hill showed that muscle twitches were completely blocked by ethanol above 6%. This concentration of ethanol inhibits glucose exits in erythrocytes by lowering the surface tension of water (Widdas & Baker, 1991).The physical chemical problems, which are involved if two energy sources contribute to the same mechanical function as proposed by Widdas & Baker (2001) can now be more clearly defined.

It is now proposed that there should be a reconsideration of the contribution of the surface energy of water in supplementing that of ATP hydrolysis in the work of muscle contraction. It is noted that this energy source was first suggested ninety years ago: that available from ATP is four and a half times smaller than the work done by the surface energy of water in a half-cycle of the red cell glucose transporter (GLUT1). Further, surface energy is a 'free' energy source, arising from cycles of water evaporation and condensation within the cells.

The mechanical energy effectively comes from the latent heat of condensation of water. Although the latent heat of evaporation comes from thermal energy of the bulk cell-water, itself derived from metabolism, there is no extra hydrolysis of ATP involved. Thus, muscle shortening would be thermally more efficient. If this mechanical concept also applies to cardiac muscle, the increase in efficiency may be vital to medical science as well as to skeletal muscle physiology.

Bernstein, J. (1908), Pflugers Arch, 122, 129-195.

Faraday, M. (1846), Literary Gazette, 20th June p. 560.

Weizsacker, V. (1914), J. Physiol. 48, 396-427.

Widdas, W. F. (1993). Biomedical Letters, 48, 15-27.

Widdas, W. F. & Baker, G. F. (1991), Cytobios, 66, 179-204.

Where applicable, the experiments described here conform with Physiological Society ethical requirements.

PC2

MODELLING OF THE ATP-INHIBITORY MECHANISM IN ATP-SENSITIVE POTASSIUM CHANNELS: INSIGHTS FROM COMPUTER SIMULATIONS OF WILD-TYPE AND GATING MUTANTS

L. Shang, P. Tammaro, S.J. Tucker and P. Proks

Oxford Centre for Gene Function, University Laboratory of Physiology, University of Oxford, Oxford, UK

ATP-sensitive potassium (K_{ATP}) channels control electrical signalling in diverse cell types by coupling cellular metabolism to potassium movement across cell membranes. Their activity is regulated by intracellular adenine nucleotides, with ATP having an inhibitory effect and MgADP having a stimulatory effect on channel activity. More recently, the state-dependency of ATP inhibition has become a matter of controversy; in particular it is unclear whether ATP interacts with the open state of the channel to induce pore closure (e.g. Enkvetchakul et al. 2001; Li et al. 2003). In order to resolve this controversy, we have simulated single-channel activity with the QuB program (Qin & Auerbach, Buffalo University, USA) using a wide range of kinetic models that incorporate both the tetrameric structure of the channel and different topologies of intraburst/interburst transitions. We next performed single-channel and macroscopic analysis of in silico single channel records to obtain ATP dependencies of dwell times and dose-response curves of K_{ATP} channel inhibition. Our results demonstrated that models which assume that stabilisation of the closed states is the sole mechanism of ATP inhibition are inconsistent with single-channel kinetics of K_{ATP} channels. We further extended our models to simulate the effects of mutations in the Kir6.2 subunit that affect gating of the unliganded channel. These results are used to discuss the possible contribution of gating and transduction mechanisms to the altered ATP sensitivity observed in these mutants.

Enkvetchakul, D., Loussouarn, G., Makhina, E. and Nichols, C.G. (2001). Biophys. J. 80:719-728

Li LH, Geng XH, Drain P (2002). J Gen Physiol 119: 105-116.

Where applicable, the experiments described here conform with Physiological Society ethical requirements.

PC3

A DYNAMIC MODEL OF pH REGULATION IN THE MYOCYTE

E.J. Crampin and N.P. Smith

Bioengineering Institute, University of Auckland, Auckland, New Zealand

We have developed a dynamical model of pH regulation and acidosis in the myocyte. Acidosis of myocardium is correlated with reduced strength of muscle contraction (Orchard & Kentish, 1990), and disturbances to heart rhythm (Orchard & Cingolani, 1994). These effects are mediated through interactions between protons (intra- and extra-cellular) and various proteins in the myocyte, which couple the regulation of pH to ionic transport, and so also affect the cellular homeostasis of other ionic species. Based on data reported by Vaughan-Jones and colleagues (Leem et al. 1999), we developed multi-state enzyme-kinetic equations describing the four transmembrane proton or acid-equivalent ion transporters (Na^+-H^+ exchange, Na^+-HCO_3^- cotransport, Cl^--HCO_3^- exchange and Cl^--OH^- exchange) and the physicochemical buffering of pH in the myocyte. We have extended the existing modelling framework for myocyte electrophysiology, calcium handling and contraction to include the pH-dependence of key sarcolemmal ion channels and transporters involved in calcium handling and electro-mechanical coupling, in particular the inhibitory effects of protons on the L-type Ca^{2+} channel, the RyR Ca^{2+} release sites of the sarcoplasmic reticulum and the Ca^{2+} pump SERCA. The model is able to reproduce data on acid loading experiments (Leem et al. 1999), and predicts time courses for key ionic species during acidosis in the beating heart, in particular rising intracellular Na+ and Ca^{2+}, and the inhibitory action of protons on

the contractile proteins. We have embedded the cellular model of acidosis into a 2-dimensional slice (Crampin et al. 2004) of the Auckland heart model (Smith et al. 2004) to investigate altered contraction and pump function arising from region of acidosis (Fig. 1). The simulation shows an altered electrical activation sequence and reduced tissue deformation in the vicinity of the region of acidosis in the left ventricular wall.
This study indicates that a computational modelling framework will provide a useful mechanism for investigating the effects of acidosis on heart function, and represents an important step towards a fully dynamic model of myocardial ischaemia.

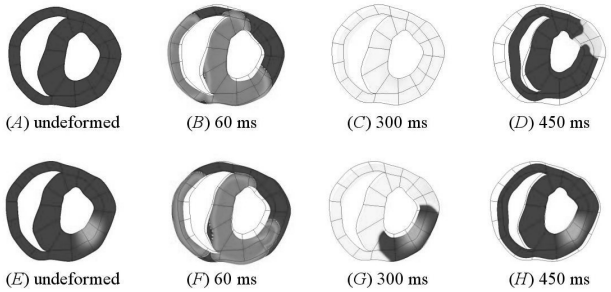

Figure 1. A tissue slice from the Auckland ventricular model (Smith et al. 2004) showing cell membrane potential and tissue deformation during normal electrical excitation (A)-(D) and with a region of acidosis in the left ventricular wall (E)-(H). The undeformed mesh is shown for reference.

Orchard CH & Kentish JC (1990). Am. J. Physiol. 258, C967-981.

Orchard CH & Cingolani HE (1994). Cardiovasc. Res. 28, 1312-1319.

Leem CH, Lagadic-Gossmann D & Vaughan-Jones RD (1999). J. Physiol. 517, 159-180.

Crampin EJ, Halstead M, Hunter P, Nielsen P, Noble D, Smith N & Tawhai M (2004). Exp. Physiol. 89, 1-26.

Smith NP, Nickerson DP, Crampin EJ, Hunter PJ (2004) Acta Numerica 13, 371-431.

Where applicable, the experiments described here conform with Physiological Society ethical requirements.

PC4

Ca^{2+} DEPENDENT ENZYME KINETICS RELATED TO INTRACELLULAR Ca^{2+} DYNAMICS IN RAT CARDIAC MYOCYTES

J. Koivumaki[1], P. Niemela[1], P. Tavi[2] and M. Weckstrom[1]

[1]Department of Physical Sciences, Division of Biophysics, and Biocenter Oulu, University of Oulu, Oulun yliopisto, Finland and [2]Department of Physiology, and Biocenter Oulu, University of Oulu, Oulun yliopisto, Finland

Signalling with intracellular enzymatic cascades is a complicated process in cardiac myocytes. Periodic, pulsatile changes in intracellular Ca^{2+} concentration have a crucial role in activation of several of these pathways. We present a mathematical model illustrating the control of enzyme kinetics in rat cardiac myocytes. The model development was based on previous work (Bhalla & Iyengar, 1999; Tavi et al. 2003, 2004). The model includes intracellular Ca^{2+} handling as well as interactions between calmodulin (CaM), calcineurin (CaN), protein phosphatase 1 (PP1) and calmodulin kinase II (CaMKII). Simulations using both the experimental calcium transients from isolated ventricular myocytes and the simulated transients indicate that the model consistently predicts time courses of enzyme activations in agreement with other available experimental data. In previous research projects (Tavi et al. 2003, 2004), we have shown this type of modelling to be useful in understanding experimental results related to CaN and CaMKII activation. The new model increases our understanding of the role of PP1 in the interaction between CaN and CaMKII and of the role of localization of CaM. Our model provides novel ways to study the enzyme cascades, e.g. the effect of durations, amplitudes and intervals of the intracellular calcium signals may be varied in the physiological range of parameters. It also makes it possible to go beyond the physiological range of stimuli and reaction parameters, which may be useful in revealing hidden aspects of signalling. Our results show what is the frequency dependence of the Ca^{2+} dependent enzyme activation. The modelling also shows the differences of enzyme signalling in the cytosol vis-à-vis the nucleus.

Bhalla US & Iyengar R (1999). Science 283, 381-387.

Tavi P et al. (2003). J Physiol 551, 5-12.

Tavi P et al. (2004). J Physiol 554, 309-320.

Supported by the Academy of Finland (to M.W.)

Where applicable, the experiments described here conform with Physiological Society ethical requirements.

PC5

MODELLING THE DISTRIBUTION OF $[Ca^{2+}]$ WITHIN THE CARDIAC T-TUBULE - EFFECTS OF Ca^{2+} CURRENT DISTRIBUTION AND CHANGES IN EXTRACELLULAR $[Ca^{2+}]$

J. Simurda[1], M. Pasek[2], G. Christe[3] and M. Simurdova[1]

[1]Department of Physiology, Faculty of Medicine, Masaryk University, 662 43, Brno, Czech Republic, [2]Institute of Thermomechanics, Czech Academy of Science - branch Brno, 616 69, Brno, Czech Republic and [3]INSERM E0219, DRDC/DVE, CENG, F-32054, Grenoble, France

To calculate the spatial and temporal distribution of $[Ca^{2+}]$ within the transverse tubules (t-tubules) of cardiac myocytes, we have developed a model described by partial differential equations. Ca^{2+} diffusion, and Ca^{2+} binding at the t-tubule membrane and/or in the t-tubule lumen were modelled for cylindrical (254 nm diameter) t-tubules of finite length. When the Ca^{2+} binding rate constants were set to 2 mM^{-1} s^{-1} (kon), 10^{-2} s^{-1} (koff) and the diffusion coefficient to 8×10^{-6} cm^2 s^{-1}, the model responded to a sudden increase of bulk extracellular $[Ca^{2+}]$ from 0 to 1 mmol/l in a way that reproduced the wave-like propagation of $[Ca^{2+}]$ along the t-tubules described by Blatter and Niggli (1998). The velocity of propagation decreased markedly with increased t-tubular length, varying between 5 and 60 μm s^{-1} in the middle of 5 to 30 μm long t-tubules. To study the effect of Ca^{2+} channel distribution (and thus of ICa-density) along the t-tubules, two separated clusters of Ca^{2+}-channels were considered (Fig. 1, upper right panel). The non-uniformity in ICa-density was reflected in non-homogeneous Ca^{2+}-depletion along the t-tubule during activation of ICa, which was inactivated with a time constant of 50 ms (Fig. 1, lower right panel). Due to the Ca^{2+}-buffering, the initial effect of Ca^{2+}-channel localization was

damped out rapidly: the initial irregularities in Ca^{2+} depletion were prominent 60 ms after activation of ICa, very small after 150 ms and absent after 300 ms. For comparison, when assuming uniformly distributed ICa transferring the same electrical charge across the t-tubular membrane (Fig. 1, left panels), the model predicts, at all times, a monotonous increase in Ca^{2+} depletion with depth along the t-tubule.

Thus Ca^{2+} binding within the t-tubules significantly affects variations of tubular [Ca^{2+}] induced both by changes in extracellular [Ca^{2+}] and by Ca^{2+} transport across the tubular membrane. We conclude that such models can provide detailed information that is neglected if the t-system is described by lumped models. This may be important because ion transport proteins may be non-uniformly distributed along the t-tubule (Scriven et al. 2000).

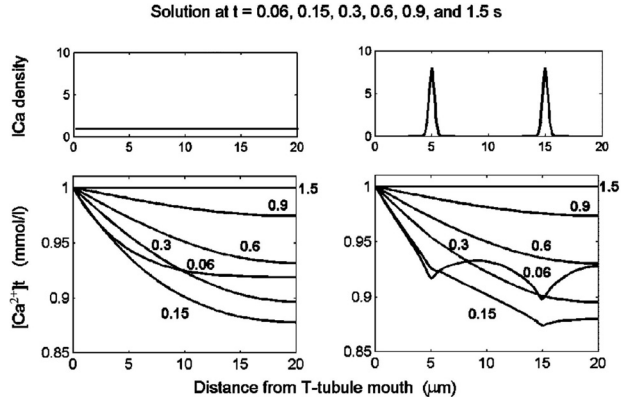

Figure 1: Depletion of Ca^{2+} in the t-tubule lumen induced by activation of ICa

Blatter LA & Niggli E (1998) *Cell Calcium* **23**:269-79.

Scriven DR *et al.* (2000) *Biophys. J.* **79**:2682-91.

Where applicable, the experiments described here conform with Physiological Society ethical requirements.

PC6

MODELLING CHANGES OF [Ca^{2+}] AND [K^+] IN THE T-TUBULES OF RAT AND GUINEA PIG VENTRICULAR MYOCYTES

G. Christe[1], M. Pasek[2] and J. Simurda[3]

[1]INSERM E0219, DRDC/DVE, CENG, F-32054, Grenoble, France, [2]Institute of Thermomechanics, Czech Academy of Science - branch Brno, 616 69, Brno, Czech Republic and [3]Department of Physiology, Faculty of Medicine, Masaryk University, 662 43, Brno, Czech Republic

The morphology of the cardiac transverse (t-) tubular system has been known for decades, but its function has received little attention. To explore the possible role of this system in the physiological modulation of electrical and contractile activity, we have developed mathematical models of guinea pig and rat ventricular cardiomyocytes in which the t-tubules are described as a single compartment (Pasek et al. 2003). The geometrical characteristics of the t-tubules, the biophysical characteristics of ion transporters, and their distribution between surface and t-tubular membranes in the models were based on available experimental data for the two species. Biophysically realistic values of mean access resistance to the tubular lumen and time constants for ion exchange with the bulk extracellular solution were included. The fraction of membrane in the t-tubules was set to 32% in the rat model (detubulation data of Brette and Orchard 2003) and to 52% in the guinea pig model (Amsellem et al. 1995). In both models, the action potential initiated by brief stimulation (1 ms, 1.5 x threshold) in current clamp is accompanied by transient K^+ accumulation (Fig. 1, grey bars) and transient Ca^{2+} depletion (Fig. 1, black bars) in the t-tubule lumen. The amplitude of these changes relative to external ion concentrations was studied at steady state stimulation frequencies of 1 to 5 Hz. In the rat model (Fig. 1, rat), Ca^{2+} depletion increased from 11.8 % to 20.8 % with stimulation frequency, while K^+ accumulation decreased from 4.3 % to 3 %. In contrast, the guinea pig model (Fig. 1, Guinea pig) exhibited a decrease of tubular Ca^{2+} depletion from 15.6 % to 7.1 % and increase of tubular K^+ accumulation from 2.5 % to 3.4 % over the same frequency range.

Thus, the relative Ca^{2+} depletion is 2-6 fold larger than K^+ accumulation, and the frequency-related changes in t-tubular [Ca^{2+}] and [K^+] are in opposite directions in the two species. Therefore, these changes are likely to play an important role in the electrical and contractile responses to altered stimulation frequency in the two species.

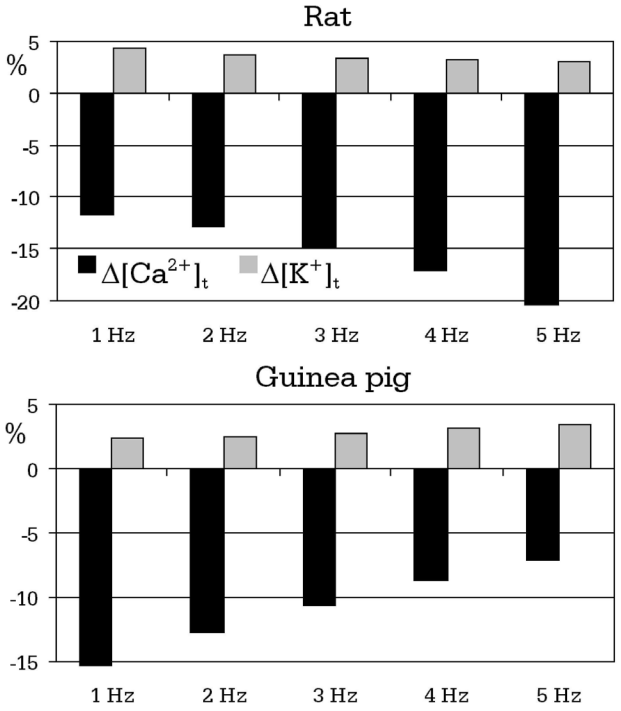

Figure 1: Transient changes in tubular [Ca^{2+}] and [K^+] ions at various frequencies, relative to external ionic concentration: rat ($[Ca^{2+}]_e$=1.2 mM, $[K^+]_e$=5.4 mM), guinea pig ($[Ca^{2+}]_e$=1.8 mM, $[K^+]_e$=5.4 mM). Note different vertical scales in the two panels.

Brette F & Orchard CH (2003) *Circ. Res.* **92**:1182-1192.

Pasek M *et al.* (2003) *Gen. Physiol. Biophys.* **22**:355-68.

Amsellem J *et al.* (1995) *Biol. Cell* :43-54.

This study was supported by grant GACR 204/02/D129 and by project AVOZ 2076919

Where applicable, the experiments described here conform with Physiological Society ethical requirements.

PC7

A COMPUTATIONAL MODEL OF THE EFFECTS OF ACIDOSIS ON INTRACELLULAR Ca^{2+} IN RAT VENTRICULAR MYOCYTES

E. Langham[1], R. Clayton[2], M. Pasek[3] and C.H. Orchard[1]

[1]School of Biomedical Sciences, University of Leeds, Leeds, UK, [2]Department of Computer Science, University of Sheffield, Sheffield, UK and [3]Department of Physiology, Masaryk University, Brno, Czech Republic

The effects of acidosis on intracellular [Ca^{2+}] (Ca_i) have been studied extensively; acidosis increases diastolic Ca_i and the amplitude of the systolic Ca_i transient, although in some studies this is preceded by a small decrease in Ca_i transient amplitude (Orchard and Kentish, 1990). It has been suggested that these changes result from the effects of acidosis on: (i) Ca^{2+} influx via Na/Ca exchange, (ii) release of Ca^{2+} from the sarcoplasmic reticulum and (iii) intracellular Ca^{2+} buffering (Orchard and Kentish, 1990; Orchard, 2004). The relative importance of each of these components is difficult to establish experimentally. We have therefore used a model of the rat ventricular myocyte based on that described by Pandit et al (2001) to investigate whether the integrated response to these changes is compatible with that observed experimentally during acidosis.

Figure 1 shows the response of the model to three effects of acidosis suggested by experimental data: (A) Increasing intracellular Na^+ from 11 mM to 15mM, by increasing background Na^+ conductance, thus altering Na^+/Ca^{2+} exchange activity, increased diastolic Ca_i and Ca_i transient amplitude. (B) Decreasing the sensitivity of the ryanodine receptor to trigger Ca^{2+}, by decreasing the rate constant for channel opening by a factor of 0.25, decreased Ca_i transient amplitude. (C) Decreasing Ca^{2+} binding to troponin-C, by increasing the off-rate of Ca^{2+} from troponin by a factor of 4.0, decreased diastolic Ca_ibut increased Ca_i transient amplitude. (D) Combining these three changes increased diastolic Ca_i and Ca_i transient amplitude. All changes were made with a time course similar to the change of intracellular pH recorded experimentally; the responses are similar to those recorded experimentally in response to acidosis, consistent with the idea that they underlie the changes of Ca_i observed during acidosis.

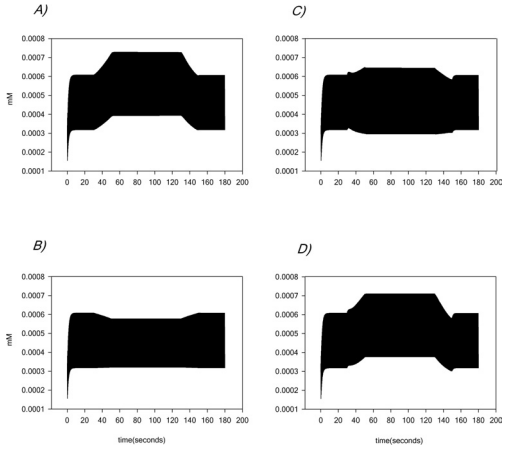

Fig 1: Ca_i during the changes described above. Each run begins with 30 s control followed by the desired change made over 20 s, followed by 80 s at the maximum level of that change. The change is then gradually reversed over 20 s followed by 30 s control.

Orchard, C.H. (2004). *J Mol Cell Cardiol* 36, 21-24.

Orchard, C.H. & Kentish, J.C. (1990). *Am J Physiol* 258, C967-981.

Pandit, S.V. et al. (2001). *Biophys J* 81, 3029.

This work was supported by the British Heart Foundation grant number PG/02/158/14785.

Where applicable, the experiments described here conform with Physiological Society ethical requirements.

PC8

CHANGES OF [Ca] IN THE T-TUBULE LUMEN DURING ACTIVITY MAY MODULATE THE INOTROPIC STATE OF RAT CARDIAC VENTRICULAR MYOCYTES

M. Pasek[1], G. Christe[2], J. Simurda[3] and C.H. Orchard[4]

[1]Institute of Thermomechanics, Czech Academy of Sciences, Brno, Czech Republic, [2]INSERM EMI 0219, DRDC/DVE, CEA, Grenoble, France, [3]Department of Physiology, Masaryk University, Brno, Czech Republic and [4]School of Biomedical Sciences, University of Leeds, Leeds, UK

The t-tubules are invaginations of the surface membrane of mammalian ventricular myocytes. The majority of trans-sarcolemmal Ca flux occurs across the t-tubule membrane (Brette & Orchard, 2003); however Ca within the t-tubules does not equilibrate instantaneously with the bulk extracellular solution (Blatter & Niggli, 1998). Thus during activity, [Ca] may change within the t-tubule lumen; this would, in turn, alter trans-sarcolemmal Ca flux.

To test this hypothesis, we used a computer model of the ventricular myocyte including a t-tubular system (Pasek et al. 2003), modified to be consistent with data from rat ventricular myocytes. The t-tubules are described as a single compartment separated from the bulk extracellular solution by the mean resistance of the tubular system. A single t-tubule is represented as a cylindrical conductor with a lumen resistance of 9.8 MΩ. The fraction of membrane within the t-tubule compartment (32 %) and the distribution of ion transport mechanisms between the surface and t-tubule membranes were set as determined using detubulation of rat ventricular myocytes (Brette & Orchard, 2003).

The action potentials in the two membranes were not significantly different. However, [Ca] within the t-tubule lumen decreased on each stimulus, and decreased cumulatively, until it reached a new dynamic steady state, with increasing stimulation rate (Fig. 1). Figure 1 also shows that Ca depletion in the t-tubule lumen was reflected in decreased sarcoplasmic reticulum Ca content and intracellular [Ca] transient amplitude (solid lines), in comparison with a ventricular cell model that did not take the t-tubules into account (dotted lines), but used the same total cell membrane capacitance and current magnitudes.

These data suggest that activity-dependent depletion of Ca within the t-tubule lumen, adjacent to the trans-sarcolemmal Ca flux pathways, may decrease the Ca load, and hence the inotropic status, of ventricular myocytes in physiological conditions.

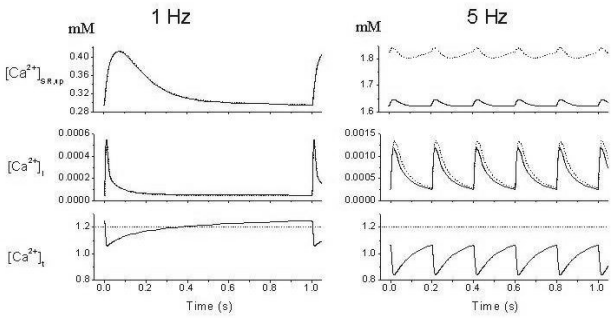

Figure 1. [Ca] in the uptake compartment of the sarcoplasmic reticulum (top), cell cytoplasm (middle) and t-tubule lumen (bottom) in the presence (solid line) and absence (dotted line) of t-tubules, during stimulation at 1 Hz (left) and 5 Hz (right) at a bulk extracellular [Ca] of 1.2 mM (indicated by the horizontal dashed line in the lower panels).

Blatter LA & Niggli E (1998). Cell Calcium 23, 269-79.

Brette F & Orchard CH (2003). Circ Res 92,1182-92.

Pasek M et al. (2003). Gen Physiol Biophys 22, 355-68.

Supported by grant GACR 204/02/D129 and project AVOZ 2076919, and by the Wellcome Trust

Where applicable, the experiments described here conform with Physiological Society ethical requirements.

PC9

MATHEMATICAL MODELLING OF ALTERNANS OF CALCIUM IN CARDIAC CELLS

T. Tao[2], S.C. O'Neill[1], M.E. Diaz[1], Y.T. Li[1], D.A. Eisner[1] and H. Zhang[2]

[1]Medicine, University of Manchester, Manchester, UK and [2]Biological Physics, UMIST, Manchester, UK

Cardiac mechanical alternans are believed to be associated with intracellular Ca alternans. Mechanisms underlying Ca alternans are unclear. We have developed a cardiac cell model with 6 μm resolution to study the roles of sarcoplasmic reticulum (SR) Ca content, ryanodine receptor (RyR) opening and Ca waves in the generation of Ca alternans. Each element has a voltage-gated L-type Ca channel, a subspace, a cytoplasm space and SR RyR channel. For each of 25 elements, mathematical equations were developed to model local intracellular Ca cycling. Inter-element coupling was via Ca diffusion between neighbouring subspaces and cytoplasm spaces. We have previously shown under voltage clamp, that small depolarising pulses produce marked alternans of systolic Ca transients (Diaz et al., 2004). We believe this is related to activation of only a few L-type channels and initiation of propagating waves of Ca release from these sites. In simulations small pulses were used to reduce L-type channel opening. To further reduce current 10 out of 25 channels were blocked by 95% in a random pattern in each pulse. Line scans of $[Ca]_i$ were plotted against time and space (Fig. 1). Local and whole cell $[Ca]_i$, SR Ca content and Na/Ca exchange current (NCX) were measured.

The large stimuli produced spatially uniform transients (not shown). The smaller pulse at first produced a very small $[Ca]_i$ transient that then alternated between large and small. This was associated with alternans of SR Ca content. Importantly, Fig. 1B shows that large releases are not spatially uniform. The small pulse activates L-type channels at only a few sites to give Ca release at these points. When SR Ca is high these release sites stimulate their neighbours and a propagating wave is initiated. With a large release a large NCX current follows depleting the SR. So, wave propagation on the next pulse is not possible and only localised Ca sparks are seen. SR refilling can then take place. The simulations are consistent with our experimental observations and show that Ca alternans can be generated and sustained through alternation of SR Ca content produced by wave propagation.

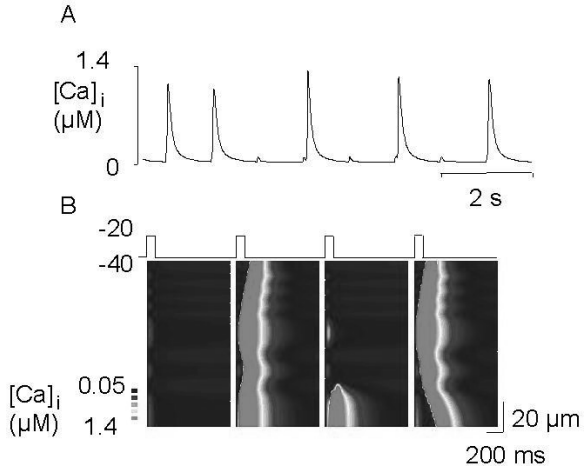

Figure 1. A. [Ca]i from a single element of the RyR cluster, pulses of 100 ms at 1 Hz were applied for the first 2 s from -40 mV to 0 mV and thereafter from -40 mV to -20 mV. B. Line scan of [Ca]i showing non-uniform nature of large releases during alternans.

Diaz, M.E., O'Neill, S.C. & Eisner, D.A. (2004) Sarcoplasmic reticulum calcium content fluctuation is the key to cardiac alternans. Circ. Res. 94, 94(5):650-6.

This work was funded by the British Heart Foundation

Where applicable, the experiments described here conform with Physiological Society ethical requirements.

PC10

THE SIMULATION OF CA^{2+}-ACTIVATED CL^- CURRENT OF CARDIOCYTES IN RABBIT PULMONARY VEIN

H.C. Seong[1], W.T. Kim[1], H. Choe[1], Y.J. Jang[1], C.S. Park[1], J.B. Youm[2] and C.H. Leem[1]

[1]Department of Physiology, University of Ulsan College of Medicine, Seoul, South Korea and [2]Department of Physiology, Inje University College of Medicine, Pusan, South Korea

We tried to simulate Ca^{2+} activated Cl^- current in isolated single cardiocytes in pulmonary vein. We could record the transiently activated current by the application three step voltage pulses (holding potential : -40 mV, -80 mV for 50 ms, 30 mV for 5 ms, 10 mV steps from -70 mV to 60 mV) and found this transient current was a Ca^{2+}-activated Cl^--current. For the simulation of this current, all information of the cellular geometry, the intracellular Ca^{2+}-regulation and the membrane ionic current systems must

be exactly specified. The mean capacitance, length, width and depth are 39.4±3.3 pF (n=30), 116.56±3.7 μm, 10.61±0.34 μm and 6.15±0.24 μm, respectively (mean±S.E.M, n=37), which suggested no existence of t-tubular system and a similar geometry to atrial myocytes (Hüser et al, 1996). Cytosolic application of 1 μM Ca2+ did not activate the Ca^{2+}-activated Cl^--current, which suggested that the cytosolic Ca^{2+} is probably compartmentalized. Na^+-Ca^{2+} exchange current amplitude was used to calculate the required subsarcolemmal Ca^{2+} concentration. Two releasable sites of the sarcoplasmic reticulum (SR) in atrial myocytes such as junctional SR and central SR were identified (Kockskämper et al., 2001). From those structural data, we composed six compartments for Ca^{2+} regulation such as cytosolic, subsarcolemmal, junctional, junctional SR, central SR and network SR. We incorporated the kinetics of ryanodine sensitive Ca^{2+} release channel based on the report (Fill et al. 2000; Györke & Györke, 1996) with the modification of the kinetics. The L-type Ca^{2+} current kinetics were reconstructed based on our data and the modified version of Shirokov et al. (1993) by Matsuoka et al. (2003). The Na^+-Ca^{2+} exchange current kinetics and SERCA kinetics of Matsuoka et al. (2003) were incorporated. For the Ca^{2+} buffers of each compartment were incoporated from the data of Bers (2002). We adjusted the amplitude of all related components and successfully simulated Ca^{2+}-activated Cl^--current. From the simulation, we found the junctional [Ca^{2+}] can increase up to hundreds μM and the subsarcolemmal [Ca^{2+}] can increase up to several tens μM. The Km value of Ca^{2+}-activated Cl^--current for Ca^{2+} may be over 50 μM.

Bers (2002) *Kluwer Academic Publishers.* **39**-62.

Fill *et al.* (2000) *J. Gen. Physiol.* **116**, 8973-8882.

Györke & Györke (1996) *Biophys. J.* **75**, 2801-2810.

Hüser *et al.* (1996) *J. Physiol.* ***494****, 641-651.*

Kockskämper et al. *(2001).* Biophys. J. ***81****, 2590-2605.*

Matsuoka et al. *(2003).* Jpn. J. Physiol. ***53****, 105-123.*

This work was supported by the grant (No. IMT2000-C3-3) from the Ministry of Information and Communication.

Where applicable, the experiments described here conform with Physiological Society ethical requirements.

PC11

MODELLING ELECTRICAL ACTIVITY OF CARDIOCYTE IN PULMONARY VEIN OF RABBIT

C. Leem[1], H. Seong[1], J. Youm[2], W. Kim[1], H. Choe[1], Y. Jang[1] and C. Park[1]

[1]Department of Physiology, University of Ulsan College of Medicine, Seoul, South Korea and [2]Department of Physiology, Inje University College of Medicine, Pusan, South Korea

Atrial fibrillation is the most prevalent arrhythmia, however, the mechanisms of development of atrial fibrillation are not yet clear. Recently the most frequent source (over 90%) of paroxysmal atrial fibrillation is located inside main pulmonary veins. We isolated the cardiocyte from the main pulmonary vein of humanely killed rabbits and found these cells can generate spontaneous action potential. More interestingly, the increase of intracellular Na^+ or Ca^{2+} accelerated the beating frequency, comapatible to atrial fibrillation (>5Hz). Therefore these cardiocytes may produce an ectopic activity for generating atrial fibrillation. We checked the electrical characteristics of these cardiocytes and tried to identify the mechanism of spontaneous action potential. Many different kinds of ionic channel activity were identified such as, I_{Na}, $I_{Ca,L}$, I_{Ks}, I_{K1}, I_{Kr}, I_{ncx}, $I_{K,ATP}$, $I_{K,ACh}$, and $I_{Cl,Ca}$. We could not identify $I_{Ca,T}$, I_{ST}, and I_f, which are main currents for pace making activity of sinoatrial node cells. We tried to make the model of these cardiocyte to identify what is the main cause of spontaneous action potential. We used and tried to reconstruct many experimental observations. The measured membrane area (3907 μm^2) was well matched to the capacitance value (39.4±3.3 pF, n=30), which suggested no existence of t-tubular system. Cytosolic application of 1 μM Ca^{2+} did not activate the Ca^{2+}-activated Cl^--current, which suggested that the cytosolic Ca^{2+} is compartmentalized. From the atrial myocytes and this experimental observations, we composed six compartments for Ca^{2+} regulation such as cytosolic, subsarcolemmal, junctional, junctional SR, central SR and network SR. We found the steady-state inactivation curve of L-type Ca^{2+} current was shifted to the negative potential which is a clear difference from ventricular myocytes. From these reconstructions, we found this shift of inactivation curve of L-type Ca^{2+} current, I_{Kr} and and Na^+-Ca^{2+} exchange current probably participates in the generation of the spontaneous action potential.

This work was supported by the grant (No. IMT2000-C3-3) from the Ministry of Information and Communication.

Where applicable, the experiments described here conform with Physiological Society ethical requirements.

PC12

DOES VISCOSITY AFFECT MYOCARDIUM MECHANICAL ACTIVITY?

L.B. Katsnelson[1], L.V. Nikitina[1], D. Chemla[2], O. Solovyova[1], C. Coirault[2], Y. Lecarpentier[2] and V.S. Markhasin[1]

[1]Institute of Immunology & Physiology of the RAS, Pervomayskaya 91, Ekaterinburg, Russian Federation and [2]Service de Physiologie, CHU de Bicetre AP-HP-Universite Paris Sud 11, Le Kremlin-Bicetre, France

To theoretically assess the effects of viscosity on cardiac mechanics, we modified our mathematical model of myocardial mechanical activity [1], which did not comprise viscous elements. Now, two dampers are included: ***VS1*** in parallel to the contractile element, and ***VS2*** in parallel to the series elastic element.

Simulation of myocardial contractions (compared to experimental data obtained from 28 rat left ventricular papillary muscles) elucidated the role of viscosity in the following experimentally observed effects:

1. time lag arising between the peak isometric force and the peak sarcomere shortening;
2. sarcomere lengthening toward its initial length in the muscle lasts longer than the muscle force relaxation in isometric twitches;
3. isotonic time-to-peak lengthening velocity is essentially load-independent (except in the medium range of afterloads, where time-to-peak may be delayed when afterload decreases).

VS1 proved to be responsible for the effects listed above as 2) and 3), whereas ***VS2*** is responsible for the singular feature of isometric contractions listed as 1) (see Figure).

We also clarified in the model how variation of the viscosity affects ino- and lusitropic myocardial function. The following characteristics were considered, first with the basic values of both kinds of viscosity, and then with a 50% reduction in either ***VS1*** or ***VS2***:
- force-length and force-velocity of contraction;
- force-velocity and force-rate of force fall of relaxation.

We conclude that the parallel viscosity ***VS1*** has a negligible effect on inotropic properties and characteristics of relaxation. The serial viscosity ***VS2*** affects neither inotropic nor lusitropic characteristics.

The latter seems noteworthy for experiments with real preparations. Indeed, in-series viscosity must be associated with the attached ends of experimental samples, i.e. it is an artificial property in respect of intact myocardium. The model predicts that this experimentally imposed condition does not affect the main myocardial mechanical characteristics obtained in experiments using such preparations.

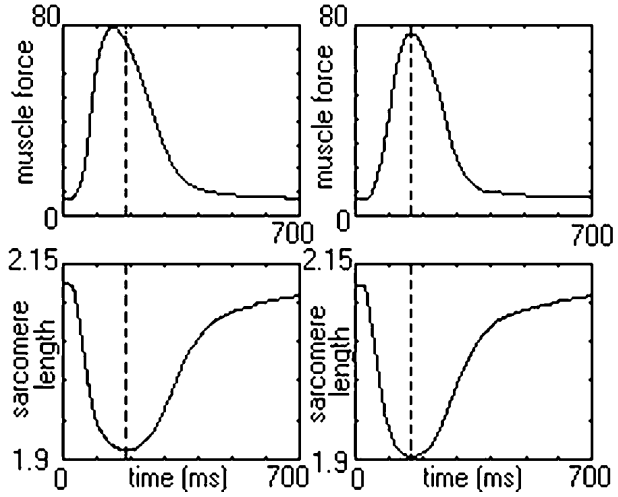

Simulation of the effect of viscosity on mismatch between the peak isometric force and sarcomere shortening. Left panels: in-series viscosity is switched on (VS2≠0). Right panels: series viscosity is switched off (VS2=0). Muscle force (top panels) in mN, sarcomere length (bottom panels) in micrometers

[1] Katsnelson LB, Markhasin VS (1996). *J Mol Cell Cardiol* **28**(3), 475-486.

The research was supported by NATO LST. CLG #975785 and RBRF Award # 03-04-48260.

Where applicable, the experiments described here conform with Physiological Society ethical requirements.

PC13

MEASUREMENT AND MODELLING OF CELL-TO-CELL PROTON TRANSMISSION IN ISOLATED VENTRICULAR MYOCYTE PAIRS FROM GUINEA PIG

P. Swietach and R.D. Vaughan-Jones

Burdon Sanderson Cardiac Science Centre, Oxford University, Oxford, UK

Local perfusion of one end of an isolated ventricular myocyte with membrane-permeant weak acids or bases results in a large and stable gradient of intracellular pH as measured using confocal imaging of carboxy-SNARF-1 (Spitzer et al. 2000). This pH_i gradient occurs because intracellular H^+ mobility is low compared with that of the weak acid/base. We have adapted this technique to both measure and model H^+ permeation across the myocardial gap junction. The proximal cell of an enzymically isolated end-to-end ventricular myocyte pair (from humanely killed guinea pig hearts) was partially perfused with Hepes-buffered Tyrode solution containing NH_4Cl (20-30mM) or Na-acetate (80-120mM). A pH_i gradient was generated down the length of the cell-pair, with a step change of pH_i occurring across the junctional region. The junctional inhibitor, α-glycyrrhetinic acid (60μM), prevented any pHi change from occurring in the distal cell (n=25), while the Na^+-H^+ exchange inhibitor, cariporide (30μM), exerted no effect, indicating that acid normally translocates the gap junction through connexin channels (Zaniboni et al. 2003). Pre- and post-junctional slopes of the pHi profile were used in conjunction with the apparent H^+ diffusion coefficient to estimate junctional acid flux, driven passively by the junctional pH_i gradient. Modelling of these parameters yielded an estimate of the apparent junctional proton permeability constant (P_H^{app}). This was converted into a mobile buffer permeability constant (P_{mob}) on the assumption that protons permeate the junction when conjugated to mobile buffers (Ref 2). At a physiological resting junctional pH of 7.04±0.02, P_{mob} was found to be $21.3\pm1.0\times10^{-4}$ cm/s (n=43). P_{mob} was also measured after cell-pairs had been acid-loaded (by uniformly prepulsing with 30mM NH_4Cl before applying the dual microstream). At a mean junctional pH_i of 6.57±0.05, P_{mob} was $14.2\pm1.6\times10^{-4}$ cm/s (n=19), a reduction of 33%, showing that a significant intracellular acidosis reduces cell-to-cell proton transmission. When cell-pairs were loaded with 100μM BAPTA-AM for 10 min, P_{mob} was reduced from $20.0\pm1.6\times10^{-4}$ cm/s (n=37) at a junctional pH_i of 7.02±0.02, to $16.8\pm2.1\times10^{-4}$ cm/s (n=25) at a junctional pHi of 6.59±0.04. Although this represents a 16% reduction, the difference was not significant (P>0.05). This suggests that over the pH_i range tested, some of the acid-inhibition of proton transmission between cells is dependent on possible changes in $[Ca^{2+}]_i$.

Spitzer KW et al (2000). Am J Physiol 278, H1371-1382.

Zaniboni et al. (2003). Circ Res 93, 726-735.

We thank the British Heart Foundation, Wellcome Trust and Overseas Research Scheme for supporting our work and KW Spitzer for providing the dual microstream apparatus.

Where applicable, the experiments described here conform with Physiological Society ethical requirements.

PC14

HODGKIN-HUXLEY TYPE COMPARTMENTAL MODELLING OF COCKROACH PHOTORECEPTORS WITH GRADED AND SPIKE RESPONSES

I. Salmela, K. Heimonen and M. Weckstrom

Department of Physical Sciences, Division of Biophysics and Biocenter Oulu, University of Oulu, Oulu, Finland

Cockroach (*Periplaneta americana*) visual system (Mote 1990) is supposed to have evolved to function especially in low light

intensity conditions. They show morphological and functional adaptations to dim environment; i.e. slow type dynamic characteristics with temporal corner frequency of about 10 Hz, green and UV sensitivity in different photoreceptors and large spatial pooling of signals in visual neuropiles. Our earlier study (Weckström et al. 1993) showed that the photoreceptors produce also spike-like potentials, one or a few on the rising phase of the graded potential response. These 'spikelets' are likely to be back-propagated action potentials originating from the axon. Since graded responses are attenuated in the thin and long axons, we suggest that the signals could be transferred in the axons mainly by action potentials.

The very thin and distant axons are not amenable to stable intracellular recordings of high quality. Hence we constructed a compartmental model with Hodgkin-Huxley type channel kinetics for simulating the conduction of the graded responses and the action potentials in the photoreceptor. The model contains several compartments for both the soma and the axon. Each compartment has a passive leak conductance and an active potassium conductance. Action potential generation sites in the axon have also an active sodium conductance. Ion channel kinetic parameters were estimated from single electrode voltage clamp recordings. Membrane specific resistance and capacitance were estimated from the measured impedance functions, and intracellular resistivity was fitted so that the attenuation of the graded responses in the model corresponded to the results of recordings from the photoreceptor soma and early axon.

Results from the model confirm that the graded responses attenuate strongly on their way from the soma to the axon terminal. The back-propagated action potentials attenuate even more, and the spike remnants in the soma match the experimental results. The spike initiation zone may be localised to the axon. The study thus provides further evidence that the cockroach photoreceptors may signal to higher visual centres in the form of action potentials.

Mote MI (1990). In Cockroaches as models for neurobiology: applications in biomedical research, ed. Huber I *et al*, pp. 203-224, Vol. II. CRC Press, Inc., Boca Raton.

Weckström M *et al.* (1993). J Neurophysiol 69, 293-296.

Where applicable, the experiments described here conform with Physiological Society ethical requirements.

PC15

Computer simulation of atherogenesis based on self-perpetuating macrophage recruitment reproduces the morphology of plaques

R.N. Poston and D.R. Poston

Centre for Cardiovascular Biology & Medicine, King, London, UK

The objective of this study was to investigate by computer simulation the hypothesis that the focal generation of an atherosclerotic plaque is a consequence of self perpetuating macrophage (Mph) recruitment.

Atherosclerosis always develops as focal plaques, in which monocytes adhere to the endothelium and enter the artery to give rise to intimal macrophages. These cells oxidise low density lipoprotein to form products, e.g. oxidised phospholipids, that can activate the endothelium to increase monocyte adhesion. Hence the focal form of the plaque may arise through self perpetuation of monocyte entry. As macrophages can release factors that promote smooth muscle accumulation, or die to produce extracellular cholesterol, the dynamics of these other important plaque components are also studied.

A computer model was written in Microsoft Visual C++, in which a computer screen represents either a) a surface view of a flattened area of an arterial wall, or b) a hardware accelerated 3D rendered model of an intact tubular artery. In a) each pixel is a cell-sized area of the wall that can be occupied by multiple smooth muscle cells (SMCs), Mphs and extracellular lipid, simulating the components that can be present through the thickening intima in vivo. Cell numbers are governed by probability functions:

1) Mph recruitment from blood monocytes at each pixel depends on an initial very low value, which increases as a function of the number of macrophages present at that pixel and those adjacent.
2) SMC accumulation depends on Mph number.
3) Mphs have a probability of death, which can depend on their number, and lipid accumulation is the direct result.
4) SMCs can optionally inhibit macrophage recruitment.

These functions are programmed by graphical interfaces. The program runs in multiple cycles, in which the cell contents at multiple randomly chosen pixels are adjusted according to the prevailing probabilities, using further randomisation to determine the result. Mphs and SMC are displayed on the screen, coded by colour for cell type and number. The part a) of the program also allows graphical display of the stacked cell components along any line on the arterial surface, simulating an intimal cross-section. The 3D image in b) is calculated from the same cellular data as in a), assuming thickening of the arterial wall proportionate to the number of cells present.

If macrophage recruitment probability is allowed to be a very steeply rising function of macrophage numbers, the program readily generates realistic lesions. Small randomly distributed fatty streak-like foci of macrophages are produced initially, which may progress or regress. Larger dome-shaped Mph rich plaques are then generated, with central fibrous cap-like central regions of SMCs. The central location of the fibrous cap and the peripheral macrophage only zone are seen as a consequence of the centrifugal growth of the plaque. Lipid accumulates centrally in the lesions. Allowing SMCs to inhibit Mph recruitment permits depletion of the central region of the lesion of Mph, as is often observed. The 3D rendered image shows a remarkable resemblance to an atherosclerotic artery in vivo.

The realistic modelling of atherosclerotic plaque morphology supports the view that plaques result from the centrifugal spread of a self-perpetuating macrophage-dependent process.

Where applicable, the experiments described here conform with Physiological Society ethical requirements.

PC16

SYNCHRONIZATION AND BURSTING IN A SIMPLE VIRTUAL GRAVID UTERUS

S. Kharche[1], A.V. Holden[1], S.W. Smye[2], S. Snowden[2], N.A. Simpson[3], R.H. Clayton[4] and J.J. Walker[5]

[1]Computational Biology Laboratory, School of Biomedical Sciences, University of Leeds, Leeds, UK, [2]Medical Physics, St. James' University Hospital, Leeds, UK, [3]Paediatrics, Obstetrics and Gynaecology Unit, Leeds General Infirmary, Leeds, UK, [4]Department of Computing, University of Sheffield, Sheffield, UK and [5]University Dept. of Obstetrics and Gynaecology, St. James' University Hospital, Leeds, UK

We caricature electrical activity of the gravid uterus by a 2D excitable medium with FitzHugh Nagumo kinetics, and estimate a pseudo-electro hysterogram (EHG) by methods of Plonsey et al. (1988).

$$\frac{du}{dt} = (\mathbf{D}(x, y)\, u')' - k\, u(u - u_a)(u - 1) - v + \mathbf{I}(x, y)$$

$$\frac{dv}{dt} = \varepsilon(G\, u - v)$$

where u and v are the variables, $'$ is differentiation with respect to space, and the input current **I**, and diffusion coefficient **D** at each point in the medium are assigned a value around a given mean using a normal distribution with standard deviation of 0.15. We consider the two cases separately (Fig 1).

For irregular **I**, the four behaviours are (*i*) no or little propagation activity (*ii*) bursting (*iii*) moderate but synchronized activity and (*iv*) high and synchronized activity.

For irregular **D** the two behaviours are either no propagation activity, or propagation above a critical $\langle \mathbf{D} \rangle$.

The pseudo EHG during bursting (region *ii*) has a low p.s.d. similar to that observed (Snowden et al. 2001). Synchronized and propagating bursting is obtained at high coupling and excitability.

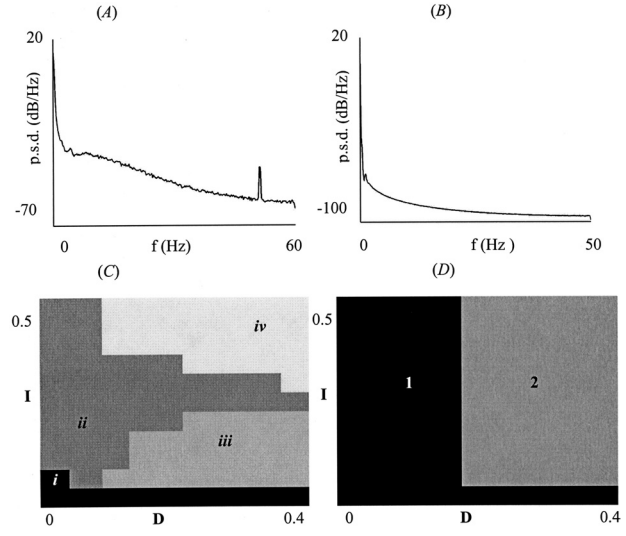

Figure 1. *A*, power spectral density (p.s.d.) normalised to peak power of clinical EHG data. At month 8 during late pregnancy (continuous line) has a low frequency component (0.2-0.45 Hz) and approximately 1 week before birth during advanced late pregnancy (dashed line) has an additional high frequency component (0.8–3 Hz). *B*, normalised p.s.d. of pseudo-EHGs from simulations where **I** was irregular. Low excitability and low coupling curve (**I** = 0.2, **D** = 0.2) peaks at 0.01 (continuous line). High excitability and high coupling curve (**I** = 0.5, **D** = 0.5) curve peaks at 0.02 (dashed line). There is an increase in high frequency power. *C*, changes in synchrony and excitability as a function of **I** and **D**, with **I** irregularly distributed. *D*, same as in *C*, but with irregular **D**.

Snowden S., Simpson N. A. B. & Walker, J. J. (2001). Physiol. Meas. **22**, 673-679.

Plonsey R. & Barr R.C. (1988). *Bioelectricity: A Quantitative Approach*, pp. 149-163. Plenum Press, New York, NY.

This work has been supported by EPSRC grant GR/R92592.

Where applicable, the experiments described here conform with Physiological Society ethical requirements.

PC17

DIMENSIONAL ANALYSIS OF COMPUTATIONAL MASS TRANSPORT IN ARTERIAL FLOWS

A.G. Radaelli[1], S.J. Sherwin[1], J. Peiro[1], D.J. Doorly[1] and T. David[2]

[1]Department of Aeronautics, Imperial College London, London, UK and [2]Department of Mechanical Engineering, University of Canterbury, Christchurch, New Zealand

Haemodynamics plays a fundamental role in atherogenesis and thrombosis. Atherosclerotic plaques are known to occur in areas of low wall shear stress and the analysis of the concentration distribution of critical blood species (oxygen, nitric oxide, etc) at these particular points may contribute to understanding the early formation of plaques.

A 2D boundary-layer analytical model of advection-diffusion-reaction at the stagnation point on the surface of the endothelium presented by David et al. (2002) has shown that the concentration distribution can be expressed in terms of a similarity function $f'(x)=(1/\phi(x,0)-1)(\mathrm{Pe}\,\mathrm{Re})^{1/3}/\mathrm{Sh}$, where $\phi(x,0)$ is the concentration along the wall (y=0), Re is the Reynolds number and Pe and Sh are the Peclet and Sherwood numbers, respectively, defined as $\mathrm{Re}=VL/\upsilon$, $\mathrm{Pe}=VL/D$ and $\mathrm{Sh}=KL/D$, where υ is the kinematic viscosity, D is the species diffusivity, K is the surface reaction rate of the species, V is a characteristic velocity and L is a characteristic length.

We present a 2D computational advection-diffusion-reaction (ADR) model of a flow around a backward facing step to analyse the early stages of atherosclerosis. For species such as oxygen, critically important in the plaque atherogenesis, $\mathrm{Pe}\geq 10^5$ and the flow solution of the Navier-Stokes equation represents the input of the ADR model. Further, we use the theoretical analysis to reduce the parameter space and to validate our results extending the dimensional analysis of the stagnation point to the whole lower wall.

Our results show the dependence of the flow regime, such as stagnation and reattachment point location, on the Reynolds number and the sensitivity of the ADR model to variations of the Peclet number. Separated flow produces internal concentration layers in the recirculation region which strongly affect the concentration distribution at the lower wall. The interpretation of our computational results shows that the similarity function $f'(x)$ analysis is applicable to the wall corresponding to the entire recirculation region for $50<\mathrm{Re}<200$ (Figs 1c and 2c). For low Re (<100), the agreement is excellent (Fig. 1c). For high Re, plots

for constant Pe illustrate a small disagreement in the recirculation region, which reflects the dependence of the characteristic concentration away from the wall $\phi(x,\infty)$ on Pe (Fig. 2c). Our results show that, for low to moderate Re, the mass transport along the entire lower wall is governed by the dimensionless parameter $(PeRe)^{1/3}/Sh$.

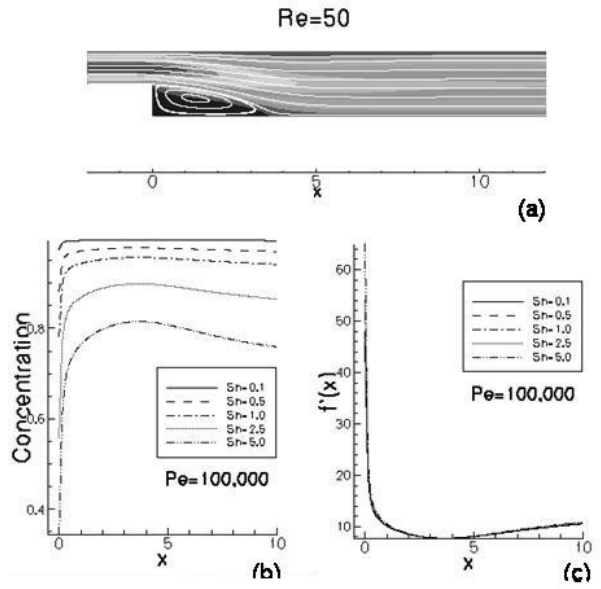

Figure 1: Re=50. (a) Flow velocity streamlines. (b) Concentration plots along the lower wall for varying Sh and Pe=100,000. (c) Similarity function f'(x) for various Sh and Pe=100,000.

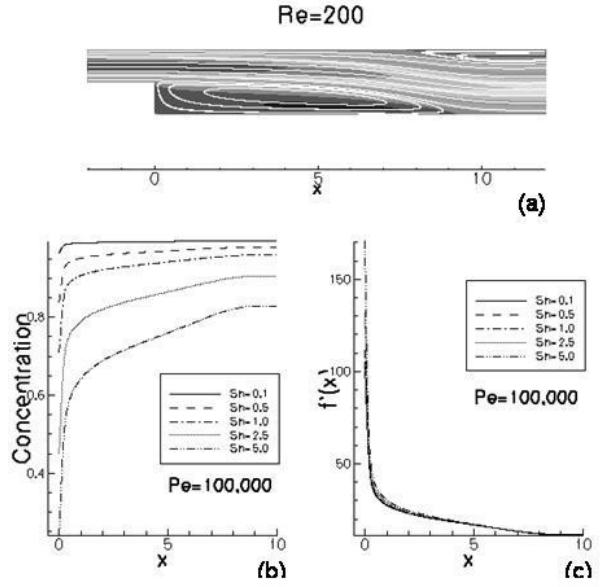

Figure 2: Re=200. (a) Flow velocity streamlines. (b) Concentration plots along the lower wall for varying Sh and Pe=100,000. (c) Similarity function f'(x) for various Sh and Pe=100,000.

David T, De Groot F & Walker PG (2002). J Theor Med 4, 95-108.

Where applicable, the experiments described here conform with Physiological Society ethical requirements.

PC18

WAVE ANALYSIS OF FLOW IN THE PALMAR ARCH

J. Alastruey, K.H. Parker, J. Peiró and S.J. Sherwin

Imperial College, London, UK

Although the topology of the human arterial system is mainly a binary tree structure, some parts are more complex. In the hands and feet the palmar and plantar arches give rise to loops. In the head, the circle of Willis gives rise to an even more complex network of arteries. Another remarkable characteristic of the arterial system is its anatomical variation.

This study is a numerical simulation of the main arteries of the human arm: brachial, ulnar, radial, palmar arch and digitals. It analyses the two topologically different networks observed after the bifurcation from the brachial artery: (a) an incomplete palmar arch and (b) a complete palmar arch. Figure 1 shows, schematically, these two possibilities. The objective is to determine if the topology of the palmar arch has a profound enough effect on flow pattern to be distinguished from pressure or flow measurements. This information may be useful in the treatment of renal patients undergoing dialysis through the arm arterial network, since blood supply may be compromised in some areas of the hand if the palmar arch is incomplete. It may also be useful to assess whether the radial artery can be harvested for use in bypass operations.

The simulation is carried out by solving the hyperbolic system of equations formed by the non-linear inviscid one-dimensional blood flow equations in compliant vessels. We separate forward and backward contributions to blood pressure and flow measured at a point by means of the method of characteristics (Parker, 1990). The system of equations is solved numerically using the discontinuous Galerkin formulation of Sherwin (2003).

When a Gaussian pressure test wave is applied at the inlet of the brachial vessel in a system with well-matched bifurcations for forward travelling waves and absorbent terminal resistances, the pressure history in the middle point of the radial artery shows the input wave with a time delay. If the palmar arch is incomplete, no further waves are observed (Fig. 1, left) and the pressure measured fully consists of forward contributions. In contrast, a set of waves is detected when we complete the palmar arch (Fig. 1, right). They are trapped waves travelling around the loop formed by the ulnar, radial and palmar arch arteries. Similar results are obtained in the ulnar artery.

We conclude that a complete palmar arch produces trapped waves that increase blood pressure and blood flow reflections at the radial artery compared with a hand with an incomplete palmar arch.

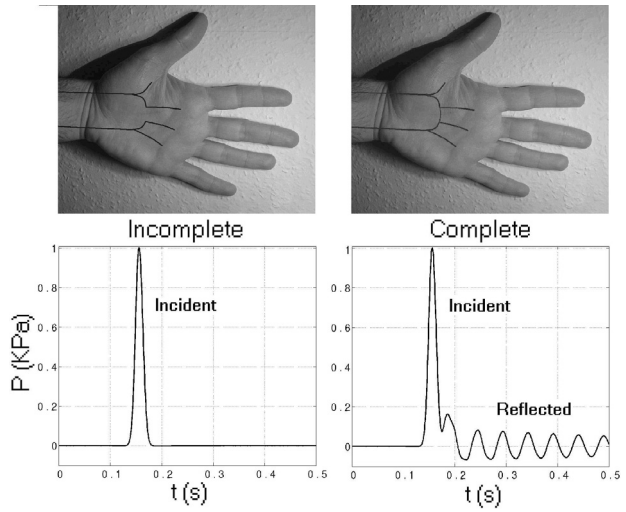

Parker KH *et.al.* (1990). *J. of Biomechanical Eng.* **112**,322-326.

Sherwin SJ *et.al.* (2003). *J. of Eng. Maths.* **47**,217-250.

Where applicable, the experiments described here conform with Physiological Society ethical requirements.

PC19

CONDUCTION BLOCK IN VIRTIUAL CARDIAC TISSUE BY DISSIPATION OF PROPAGATION FRONTS

V.N. Biktashev[1] and I.V. Biktasheva[2]

[1]Department of Mathematical Sciences, University of Liverpool, Liverpool, UK and [2]Department of Computer Sciences, University of Liverpool, Liverpool, UK

Propagation failure is an important factor in the initiation of re-entrant arryhthmias, and can play a significant role in their break-up or self-termination (Biktasheva et al 2003). One mechanism for propagation failure is accumulation of Na inactivation, which leads to inward current insufficient to maintain propagation. Phenomenologically, this mechanism is seen as a loss of the sharp gradient of the action potential profile, or "dissipation" of the propagation front (DPF) (Biktashev 2002).
DPF cannot be obtained in the FitzHugh-Nagumo caricatures of excitation, in which there is only one fast variable, but is seen in ionic models for excitation and its propagation. We have analysed the structure of Hodgkin and Huxley (1952), Noble (1962) and Courtemanche et al (1998) ionic models, identified small parameters that appear in those models in non-standard ways, and developed an asymptotic approach based on these small parameters. Further simplifications have been achieved by appropriate approximation of nonlinear functions in the models. Contrary to common belief, the fast Na current inactivation gating variable h is not necessarily slow compared to the transmembrane voltage V during the upstroke of the propagating action potential. Interplay between V and h is responsible for the DPF. We suggest a simplified model, which emerges from the asymptotic analysis, and considers V and h as equally fast variables. This model reproduces DPF and admits analytical study. In particular, it yields conditions for the DPF. This interpretation can be applied to explain the breakup and self-termination of re-entrant waves in detailed realistic ionic models. FitzHugh-Nagumo type caricatures, although successfully describing successfull propagation, fail to correctly describe propagation failure. Thus using such models to describe processes involving initiation, block of propagation or re-entrant waves in cardiac tissue may misrepresent most important features. The new simplified model or its analogue should be used instead.

Biktashev VN (2002) Phys Rev Lett 89, 168102

Biktasheva IV et al. (2003) Int J of Bifurcation and Chaos 13, 3645-3655.

Courtemanche M et al. (1998) Am J Physiol-Heart C 275, H301-H321.

Hodgkin AL & Huxley AF (1952) J Physiol 117, 500-544.

Noble D (1962) J Physiol 160, 317-352.

Thanks to A.V. Holden for helpful advice. Supported by grants from EPSRC (GR/R28935, GR/S43498, GR/S75314) and MRC (G0000315).

Where applicable, the experiments described here conform with Physiological Society ethical requirements.

PC20

MECHANICAL TERMINATION OF RE-ENTRANT EXCITATION IN A 2D VENTRICULAR TISSUE MODEL

A. Garny and P. Kohl

Department of Physiology, University of Oxford, Oxford, UK

Mechanical stimuli may trigger or terminate cardiac arrhythmias. This 'duality' is similar to that of electrical stimulation, which currently is the intervention of choice for cardiac resuscitation. It is interesting to note that only 4% of the current, applied externally for ventricular defibrillation, actually traverses the cardiac muscle (Lerman et al. 1990). This requires very high energies for resuscitation (150-300 J). Mechanical interventions, such as the pre-cordial thump (PT), offer a low-energy alternative, where stimuli of less than 1 J may trigger ectopic ventricular excitation, and impacts of 4-8 J may terminate ventricular tachycardia (VT) and fibrillation. PT is understood to be a relatively safe intervention, with the exception of pre-existing severe anoxia of the myocardium.
The effect of PT on cardiac electrophysiology is based on mechano-electric feedback, whereby mechanical stimuli are translated into increased open probability of cardiac stretch-activated channels (SAC, for review see Kohl et al. 1999). There are two main SAC populations: cation non-selective (SACNS, reversal potential near -10 mV) and K+ selective (SACK, reversal potential near -95 mV) (Craelius et al. 1988; van Wagoner, 1993). One representative of SACK is the ATP-inactivated K+ channel, which is mechanically-activated and ligand-inactivated. Interestingly, reduction in ATP content sensitizes this channel to mechanical stimulation (van Wagoner, 1993), and we propose that this may explain the reduced utility of PT in the ischaemic heart.
We simulated VT either as a single spiral wave or as figure-of-eight reentry, using a 2D ventricular model (Garny & Kohl, 2004). In short, a 2.5×2.5 cm mesh containing 63,001 ventricular cells was implemented. Re-entrant excitation was generated via localised S1-S2 stimulation protocols, and PT was simulated by brief (5 ms) activation of SACNS and SACK in variable ratios. Our results show that activation of SACNS terminates re-entry via depolarisation of cells in the excitable gap. Shifting the mod-

elled stretch-effect from SACNS only towards increasing co-activation of SACK (to represent ischaemic conditions with loss of ATP-dependent channel inactivation) decreased the efficacy of defibrillation. This is caused by the progressive shift towards a more negative reversal potential of the 'net stretch-induced current'. As a consequence, resting cells in the excitable gap are depolarised to a lesser extent, while action potential duration of excited cells is reduced. The former has no lasting effect on the excitable gap, while the latter temporarily reduces electrical cycle length, thereby facilitating re-entry. The increasing contribution of SACK may explain why PT is less efficient in hypoxic conditions, which is now subject of experimental validation.

Lerman BB et al. (1990). Circ Res 67, 1420-1426.

Kohl P et al. (1999). Prog Biophys Mol Biol 71, 91-138.

Craelius W et al. (1988). Biosci Rep 8, 407-414.

van Wagoner DR (1993). Circ Res 72, 973-983.

Garny A & Kohl P (2004). Ann NY Acad Sci 1015, 133-143.

Supported by the UK Biotechnology and Biological Sciences Research Council.

Where applicable, the experiments described here conform with Physiological Society ethical requirements.

PC21

SPATIAL DISPERSION OF REPOLARISATION AND VULNERABILITY TO RE-ENTRY IN CARDIAC TISSUE: A MODEL STUDY

R. Clayton[1] and A.V. Holden[2]

[1]Department of Computer Science, University of Sheffield, Sheffield, UK and [2]School of Biomedical Sciences, University of Leeds, Leeds, UK

Re-entrant arrhythmias are more likely to be induced in cardiac tissue with regional differences in action potential duration (APD). However, electrotonic current flow during repolarisation can mask regions with prolonged or shortened APD, and so measured APD dispersion may not reflect intrinsic regional differences in repolarisation.

In this study we used a virtual cardiac tissue to investigate how intrinsic regional differences in repolarisation can influence both measures of APD dispersion and vulnerability to re-entry following a premature stimulus. We used the LuoRudy1 model for ventricular cells (Luo and Rudy 1991) in which repolarisation is dominated by a single K^+ current. We set up 60 x 60 mm 2D virtual tissues (Clayton 2001) in which the central 40 x 40 mm region was heterogenous and made up from square regions with alternating short and long APD given by high (0.4 mS cm^{-2}) and low (between 0.1 and 0.3 mS cm^{-2}) maximal K^+ conductance (gKmax) respectively. We fixed gKmax in the surrounding tissue to be 0.4 mS cm^{-2}. We varied (i) the spatial scale of heterogeneity between 20 mm and 5 mm, (ii) gKmax of long APD regions between 0.1 and 0.3 mS cm^{-2}, and (iii) the diffusion coefficient from 0.1 cm^2 ms^{-1} to 0.05 and 0.2 cm^2 ms^{-1}. We measured the range of APD in each of these virtual tissues (APD dispersion) during pacing along one edge at intervals of 500 ms, and also the vulnerability to re-entry by a premature stimulus delivered along the same edge.

The results are shown in the table. As the spatial scale of regional differences increased, both APD dispersion and the width of the vulnerable period increased in a linear fashion. Increasing gKmax in the long APD regions (i.e. reducing APD in these regions) resulted in reduced APD dispersion and a narrower vulnerable window. Increasing and decreasing the diffusion coefficient by a factor of two also decreased and increased APD dispersion respectively. Overall there was a well correlated linear relationship between APD dispersion and width of the vulnerable window.

We conclude that although electrotonic effects can mask intrinsic regional differences in repolarisation, they also act to narrow the vulnerable period for re-entry. Thus APD dispersion provides a good estimate of vulnerability to re-entry.

Spatial scale (mm)	APD max (ms)	APD dispersion (ms)	APD standard deviation (ms)	Vulnerable window (ms)
5	231	48	6.7	31
10	253	70	9.0	56
20	285	102	14.5	86

Luo C-H. & Rudy Y. (1991). *Circ.* **68**, 1501-1526

Clayton RH. (2001) *Phys. Meas.* **22**, R15-R34

This work was funded in part by the British Heart Foundation (BS98001)

Where applicable, the experiments described here conform with Physiological Society ethical requirements.

PC22

INDUCTION OF AUTORHYTHMICITY IN VIRTUAL VENTRICULAR MYOCYTES AND TISSUE

A.P. Benson[1], W.C. Tong[1], A.V. Holden[1] and R.H. Clayton[2]

[1]Computational Biology Laboratory, School of Biomedical Sciences, University of Leeds, Leeds, UK and [2]Department of Computer Science, University of Sheffield, Sheffield, UK

Autorhythmicity was initiated in modified virtual ventricular cells and tissues of the Luo-Rudy (LRd00) family (Faber, 2000) by (1) $[Ca^{2+}]_i$ oscillations due to $[Na^+]_i$ overload and (2) block of the time-independent potassium current I_{K1}.

The voltage-clamped (dV/dt = 0, V = -80 mV) calcium subsystem at low levels of $[Na^+]_i$ has stable, steady-state $[Ca^{2+}]_i$ (Fig. 1). For $[Na^+]_i$ just above 14 mM, very low rate $[Ca^{2+}]_i$ oscillations emerge. As $[Na^+]_i$ is further increased to 16 mM, the period of the oscillations decreases to 0.65 s. In a modified LRd00 endocardial cell (100% inhibition of $I_{Na\text{-}K}$, two-fold increase of $I_{ns(Ca)}$ conductance, $CSQN_{th}$ = 7 mM, initial $[Na^+]_i$ = 20 mM and $[K^+]_i$ = 125 mM), these $[Ca^{2+}]_i$ oscillations drive sub-threshold voltage oscillations that lead to spontaneous action potentials.

Down-regulation of g_{K1}, the maximum conductance of I_{K1}, can induce autorhythmicity in ventricular cells (Miake *et al.*, 2002). Reducing fractional g_{K1} to about 0.3 in LRd00 induced low-rate membrane potential oscillations. With complete block of I_{K1} the cells oscillate with periods ranging from 308-369 ms (Fig. 1). Qualitatively similar results are found with the model of ten Tusscher *et al.* (2004) for human virtual ventricular cells, with oscillations emerging at fractional g_{K1} = 0.078 and a period of 0.8 s with complete I_{K1} block.

The large decrease in the period of the $[Ca^{2+}]_i$ and voltage oscillations close to their emergence at a bifurcation suggests homoclinic rather than Hopf bifurcations.

For all cell types, the minimal length of $[Na^+]_i$ overloaded tissue required for the initiation of propagating autorhythmic activity in 1-D homogeneous tissue strands was 1.6 mm. For reduced I_{K1}, the minimal length was 5.2 mm in 1-D homogeneous strands and the minimal radius was 3.8 mm in 2-D homogeneous tissues.

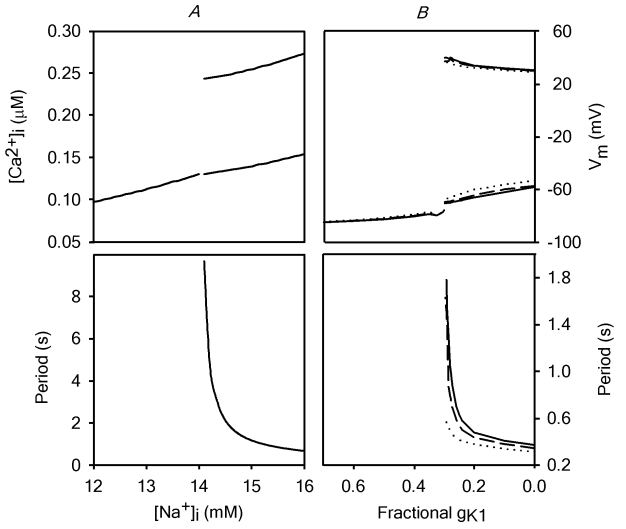

Figure 1: Bifurcation diagrams (top) showing steady states and oscillation amplitudes of (A) $[Ca^{2+}]_i$ in the LRd00 calcium subsystem with $[Na^+]_i$ as the bifurcation parameter and (B) membrane potential in epicardial (solid line), M (dotted line) and endocardial (dashed line) LRd00 cells with fractional g_{K1} as the bifurcation parameter. The corresponding periods of the oscillations are also shown (bottom).

Faber G.M. (2000). http://www.cwru.edu/med/CBRTC/LRdOnline/LRdModel.htm

Miake J. *et al.* (2002). *Nature* **419**, 132-133.

ten Tusscher K.H.W.J. *et al.* (2004). *Am. J. Physiol.* **286**, H1573-1589.

Supported by the Medical Research Council (G74/63) and the British Heart Foundation (FS/03/075/15914).

Where applicable, the experiments described here conform with Physiological Society ethical requirements.

PC23

EFFECTS OF CLASS III ANTIARRHYTHMIC DRUGS ON VULNERABLE PROPERTIES OF VIRTUAL VENTRICULAR TISSUE

O.V. Aslanidi[1], N.T. Srinivasan[2] and A.V. Holden[1]

[1]School of Biomedical Sciences, University of Leeds, Leeds, UK and [2]School of Medicine, University of Leeds, Leeds, UK

In contrast to most Class III antiarrhythmic drugs that exhibit proarrhythmic side effects, amiodarone has been found effective and relatively safe. However, the electrophysiological mechanisms underlying the low arrhythmogenecity of amiodarone are poorly understood. This study compares electrophysiological properties of virtual ventricular tissues treated with amiodarone and d-sotalol, a Class III drug known to be proarrhythmic. A one-dimensional virtual ventricular wall is constructed based on the Luo-Rudy family of models for endocardial, M- and epicardial cells (Gima & Rudy, 2002). The effects of amiodarone (Sicouri *et al.* 1997) and d-sotalol (Akar *et al.* 2002) are incorporated as changes in the maximal conductances for the fast component of the potassium current I_{Kr} (the primary target for the Class III drug action) and the calcium current $I_{Ca,L}$, which reproduces the action potential duration (APD) changes in the three cell types. Results of computer simulations with the virtual wall are summarized in Fig. 1. d-Sotalol increases the transmural dispersion of repolarization in the wall by predominant increase of APD in M-cells, as seen by Akar *et al.* (2002). This widens the vulnerable window (VW) in the endo- and epicardial regions, where uni-directional block persists until the M-cell region is fully repolarized. Amiodarone, however, decreases the dispersion of repolarization, as seen by Sicouri *et al.* (1997), by prolonging APD in endo- and epicardial cells and decreasing APD in M-cells, which results in a narrow VW similar to that of a normal tissue. We conclude that the electrophysiological explanation for the safety of amiodarone in comparison to other Class III drugs lies in relatively low dispersion of repolarization leading to narrow VW, and hence, low probability of uni-directional block and initiation of re-entry in the ventricular wall.

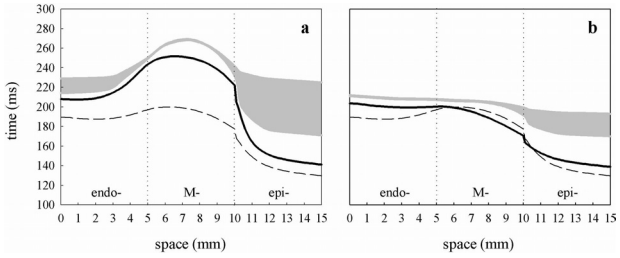

Figure 1. Effects of d-sotalol (a) and aniodarone (b) on the virtual ventricular wall. Spatial distributions of APD through the normal wall (dashed line) and the wall treated by drugs (solid lines) are shown along with the respective VWs (gray areas). Drug effects are modelled by differential blocking of I_{Kr} and $I_{Ca,L}$ in endo-, M- and epicardial cells: for the d-sotalol model I_{Kr} is depressed by 40% in endo-, by 100% in M-cell and by 65% in the epicardial region; for the amiodarone model I_{Kr} is uniformly depressed by 50% throughout the wall and $I_{Ca,L}$ is depressed by 40% in the M-cell region.

Gima K & Rudy Y. (2002). *Circ Res* **90**, 889-896.

Sicouri S *et al.* (1997). *J Cardiovasc Electrophysiol* **8**, 1269-1279.

Akar FG *et al.* (2002). *Circulation* **105**, 1247-1253.

This research was funded by the MRC and EPSRC.

Where applicable, the experiments described here conform with Physiological Society ethical requirements.

PC24

INSIGHTS INTO SICK SINUS SYNDROME CAUSED BY MUTATION OF THE CARDIAC SODIUM CHANNEL GENE

S. Inada[1], H. Zhang[2], H. Honjo[3], D. Escande[4] and M.R. Boyett[1]

[1]University of Leeds, Leeds, UK, [2]University of Manchester, Manchester, UK, [3]Nagoya Univerity, Nagoya, Japan and [4]Faculte de Medicin, Nantes, France

In the heart, sodium ion channels play a major role in the initiation, propagation, and maintenance of normal cardiac rhythm.

Sick sinus syndrome is an arrhythmia phenotype resulting from sinoatrial (SA) node dysfunction. Recently, it has been linked to mutations in the cardiac sodium channel gene, SCN5A (Benson et al. 2003). In this study, we investigated the functional effects of the mutations using computer simulation. We developed a one dimensional model of the SA node and neighbouring atrial muscle with wild-type (WT) or mutant SCN5A channels. The SA node and atrial muscle cells were simulated using the models of Zhang et al. (2000) and Ramirez et al. (2000), respectively. Figure 1A illustrates action potentials from all cells (50 SA node cells and 50 atrial cells) in the model under control conditions (WT channel) and the propagation of the action potential from the centre of the SA node to the atrial muscle is shown. Figure 1B illustrates the activation time of each cell (open squares). To simulate the effects of the mutations, the voltage dependence of inactivation of the sodium current (I_{Na}) was shifted by -10 mV, the time constant of inactivation of I_{Na} was increased three times, and the sodium conductance was decreased by up to 25%: when the sodium conductance was decreased by just 5% the conduction velocity in the SA node was decreased by 36% (Fig. 1B, filled squares); when the sodium conductance was decreased by 30% atrial stand-still occurred (data not shown). In a $SCN5A^{+/-}$ mouse, as well as a downregulation of SCN5A, there is an upregulation of L-type calcium channel genes (unpublished data). If this is translated into an increase in the L-type calcium current, it could be a compensatory mechanism, because Fig. 1B (circles) shows that a 30% increase in the L-type calcium channel conductance rescued sinoatrial conduction when the sodium conductance was decreased by 30%. These results suggest that the mutations in SCN5A may contribute significantly to SA node dysfunction.

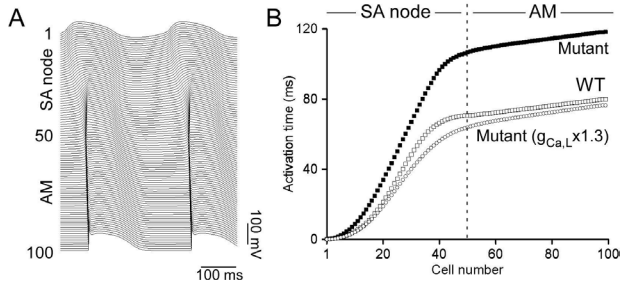

Figure 1. Activation time of the 100 cells in the one dimensional model. AM, atrial muscle.

Benson DW *et al.* (2003). *J Clin Invest* **112**, 1019-1028.

Zhang H *et al.* (2000). *Am J Physiol* **279**, 397-421.

Ramirez RJ *et al.* (2000). *Am J Physiol* **279**, 1767-1785.

Where applicable, the experiments described here conform with Physiological Society ethical requirements.

PC25

EFFECTS OF AGEING ON THE ELECTRICAL ACTIVITY OF THE SINOATRIAL NODE

Y. Zhao[2], H. Dobrzynski[1], A.V. Holden[1], M.R. Boyett[1] and H. Zhang[2]

[1]School of Biomedical Sciences, University of Leeds, Leeds, W. Yorkshire, UK and [2]Biological Physics, UMIST, Manchester, UK

In the human and other mammals, the functioning of the sinoatrial node (SAN) declines with age. A key feature is a slow down in the intrinsic heart rate (i.e., increase of the pacemaking cycle length) (Alings and Bouman, 1993). Experimental data has shown that ageing is associated with both a decrease in the SAN myocyte population (Shiraishi et al., 1992) and a possible reduction in Na+ channel expression (Alings and Bouman, 1993). It is unclear how these changes affect the pacemaker activity of the SAN.

In this study, we have constructed an anatomical model of the SAN: a section through the rabbit SAN was discretised (resolution, 35 μm) to generate a two-dimensional discrete lattice model. Each node of the lattice is represented by a model of a SAN or atrial cell as appropriate (Zhang et al., 2000). In the SAN, Cm (cell capacitance) changes from 20 pF in the centre to 65 pF in the periphery and ionic current densities are functions of Cm (Zhang et al., 2000). Each node is electrically connected to its neighbours with a junctional conductance of 25 nS (SAN-SAN or SAN-atrial) or 175 nS (atrial-atrial). In simulations, the electrical connection length (L) at the border between the SAN and atrium varied between 0.4 mm to 2.2 mm. The decrease in myocyte population (nodes made either empty or non-excitable) varied between 5-20 % and was randomly distributed across the SAN tissue. The Na+ current density in the SAN was reduced by 20-100 %. Cycle length was measured as the time interval between two successive action potentials recorded from the atrium.

A decrease of 10 % in the SAN myocyte density increased the pacemaking cycle length by 10 % when L=1.0 mm, and 20 % when L= 1.2 mm. Reduction of Na+ current density by 50 % increased the cycle length by 14 % when L=1.0 mm or 1.2 mm. 100 % reduction of Na+ current density did not abolish the pacemaker activity, but caused the SAN to fail to drive the atrium - the phenomenon of SAN exit block. When considered together, myocyte loss and reduction of Na+ current density slowed down the pacemaker activity additively.

We conclude that aging induced changes in the SAN myocyte population and SAN Na+ channel density could contribute to the slow down of the pacemaker activity.

Alings, A.M.W., Bouman, L. N. (1993). Europ.Heart J. 14,1278-1288.

Shiraishi, I., Takamatsu, T., Minamikawa, T., Onouchi, Z., Fujita, S. (1992). Circulation 85, 2176-2184.

Zhang, H., Holden, A.V., Kodama, I., Honjo, H., Lei, M., Varghese, T., Boyett, M.R. (2000). Am. J. Physiol., 279, 397-421

Supported by BHF and EPSRC.

Where applicable, the experiments described here conform with Physiological Society ethical requirements.

PC26

3D ANATOMICAL AND ELECTROPHYSIOLOGICAL MODEL OF HUMAN SINOATRIAL NODE AND ATRIA

G. Seemann[1], F.B. Sachse[2], O. Doessel[1], A.V. Holden[3], M.R. Boyett[3] and H. Zhang[4]

[1]Institute of Biomedical Engineering, University Karlsruhe (TH), Karlsruhe, Germany, [2]Nora Eccles Harrison Cardiovascular Research and Training Institute, University of Utah, Salt Lake City, UT, USA, [3]School of Biomedical Science, University of Leeds, Leeds, LS2 9JT, UK and [4]Dept. of Biological Physics, UMIST, Manchester, M60 1QD, UK

We constructed a biophysically detailed and anatomically accurate computer model of human atria that incorporates both

structural and electrophysiological inhomogeneities. The 3D geometry was extracted from the Visible Female dataset. The sinoatrial node (SAN) and atria, including crista terminalis (CT), pectinate muscles (PM), appendages (APG) and Bachmann's bundle (BB) were segmented using interactive deformable meshes. Fibre orientation in the bundles was set to local longitudinal direction.

Ionic models based on Courtemanche *et al.* (1998) were used for describing cellular electrophysiology of all tissue types. The ionic channel conductances of I_{to}, $I_{Ca,L}$ and I_{Kr} for PM, CT and BB were modified (Tab) to reproduce the action potential duration distributions of Feng *et al.* (1998).

Pacemaker activity in the SAN was reproduced by removing I_{K1}, including I_f and $I_{Ca,T}$, and modifying further channel properties using formulations of Zhang *et al.* (2000). Anisotropic propagation was computed with a monodomain approach using the finite element method.

The excitation was first initiated in the centre of the SAN (Fig 1A), then conducted preferentially towards the atrioventricular region via the CT (Fig 1B) and afterwards spread over the right atrium along the PM (Fig 1C). Earliest activation of the left atrium was in the region of BB and excitation spread over to the appendage (Fig 1D). The conduction velocities were 60 cm/s for atrium, 120 cm/s for CT, 140 cm/s for PM, and 110 cm/s for BB at a frequency of 63 bpm.

The simulation demonstrates the important role of anatomical and electrophysiological heterogeneity for a realistic propagation of excitation in the atrium. The preferential conduction towards CT and along PM is consistent with clinical endocardial mapping.

(nS/pF)	PM	CT	APG
$g_{to,max}$	0.1652	0.2115	0.1123
$g_{Ca,L,max}$	0.1238	0.2067	0.1312
$g_{Kr,max}$	0.0294	0.0294	0.0294

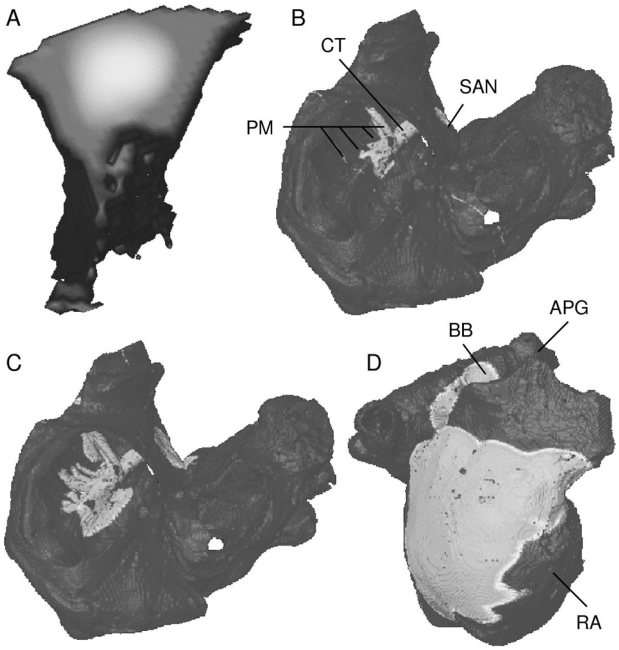

Figure 1: Gray-coded transmembrane voltage during excitation propagation in human atria. (A) SAN visualised only: Activation starts in the centre of the SAN; (B+C) View trough valves: Excitation spreads along CT and PM; (D) Lateral view: Right atrium and left via BB gets activated.

Visible Human Project: www.nlm.nih.gov/research/visible/visible_human.html

Courtemanche M *et al.* (1998). *Am J Physiol*, **275**, H301-H321

Feng J *et al.* (1998). *Circ Res*, **83**, 541-551

Zhang H *et al.* (2000). *Am J Physiol*, **279-1**, 397-421

Supported by DFG (SFB414) and EPSRC (GR/S03027/01)

Where applicable, the experiments described here conform with Physiological Society ethical requirements.

PC27

A NEW MODEL FOR RECTIFIED GLUCOSE UPTAKE INTO HUMAN BRAIN REQUIRING HEXOKINASE COUPLED TO GLUTS AT THE ABLUMINAL SIDE OF THE BLOOD BRAIN BARRIER.

R.J. Naftalin[1], J. Dunn[2], S. Amiel[3] and P. Marsden[2]

[1]Physiology, King's College London, London, UK, [2]Clinical PET centre, Guy's, King's and St Thomas' School of Medicine, London, UK and [3]Diabetic Unit, King's College Hospital, Denmark Hill, London, UK

The conventional model of glucose transport into brain assumes unregulated symmetrical passive transport across the blood brain barrier (BBB) defined by global Michaelis-Menten parameters (Kt = 5-10mM; Vmax 1μmol/g/min). Steady-state [glucose] = 1mM in the brain extracellular fluid (ecf) is maintained by removal of glucose by brain metabolism (Gruetter et al. 1998). The model predicts that glucose flow between blood and ecf is 70% maximal. However, local stimulation can raise regional brain glucose metabolism by at least 100% above basal rates and dialysis studies show only small decreases in ecf [glucose] on stimulation of brain metabolism (McNay, McCarty & Gold, 2001). These findings indicate that glucose transport across the BBB is seemingly more responsive to brain metabolism than the model permits.

Hexokinase co-localizes with glucose transporters (GLUTs) at the luminal and abluminal surfaces of the BBB, including endothelial and astroglial layers. GLUTs and hexokinase are more abundant on the abluminal surface. Hexokinase retards glucose exit from glia to ecf (McAllister et al., 2001). Glucose-6-phosphatase (G6P) is also present within glia, (Bell et al., 1993) thereby permitting glucose regeneration from G6P and its accumulation within the cytosol.

Cytosolic glucose accumulation in glia and endothelia retards net uptake across the endothelial luminal membrane. Glucose exit across the glial abluminal membrane is reduced by conversion to G6P via membrane-bound hexokinase. Reduction in ecf [glucose] induced by brain metabolism increases the glucose concentration gradients across both luminal and abluminal membranes, thereby raising net flux into brain.

Modelling these relationships with a fast simulation program, (Berkeley Madonna, www.berkeleymadonna.com), shows that regulation of BBB glucose flow depends on the extent of its accumulation within the cytosol. Reversible phosphorylation of 2-deoxy 2-fluoro-D-glucose (2FDG) in glia leads to more rapid and greater accumulation in brain than the non-metabolised, 3-O-methyl-glucoside (3-OMG).

When matched with PET scans of human brain, the model simulations are consistent with these predictions in both euglycaemic and hypoglycaemia conditions.

Bell, J. E. et al., (1993) Neuropathol. Appl. Neurobiol. 19 429-35.

Gruetter, R; Ugurbil, K. and Seaquist, E.R. (1998) J. Neurochem. 70, 397-408.

McAllister, M.S. et al., (2001) Brain Res. 904, 20-30.

McNay, E.C.; McCarty, R.C., and Gold, P.E. (2001) Neurobiol. Learn. Mem. 75, 325-37.

Supported by the Juvenile Diabetes Research Foundation.

Where applicable, the experiments described here conform with Physiological Society ethical requirements.

PC28

PRESENCE AND ABSENCE OF HARMONICS IN FFT-BASED COHERENCE ESTIMATION OF NEUROMUSCULAR COUPLING IN TREMOR

S. Wang, X. Liu, T.Z. Aziz and J.F. Stein

University Laboratory of Physiology, University of Oxford, Oxford, UK

Fast Fourier transform (FFT)-based coherence estimation is widely used for investigating neuromuscular coupling in tremor. The significant coherence was often found not only at the tremor frequency but the harmonic frequencies as well. It is necessary to differentiate the genuine physiological component from the harmonics.

We investigated the factors contributing to generation of the significant coherence estimates at the harmonic frequencies using simulated signals and physiological signals of electromyographys (EMGs) of the forearm extensor/flexor and oscillatory local field potentials (LFPs) of the subthalamic nucleus (STN) in Parkinsonian tremor. Rhythmic pulses varied in duration simulating the envelope signal in tremor EMGs and sine waves varied in waveform and level/frequency distribution of added noise simulating the tremor signals in the STN LFPs were formed. With ethics committee approval, tremor-related EMGs and STN LFPs were recorded from the Parkinsonian patients following deep brain stimulation surgery. Coherence estimation was computed between the simulated and physiological signals. The effects of pulse duration, waveform, noise level and frequency distribution were compared on the coherence results of a range of paired signals. Our results of the simulated signals showed that (1) although the signal of rhythmic pulses was significantly distorted from the perfect sine wave, which generates harmonics on the power spectrum (the shorter the duration, the more harmonic peaks appeared with lower power). This did not significantly influence the amplitude of harmonic component in the coherence estimation; (2) in comparison with near perfect sine wave, the half-wave simulated signal significantly increased the harmonic component in both number and coherence value; and (3) added white-noise significantly decreased the coherence value of harmonics, whilst the noise distributed in a particular frequency range selectively decreased the coherence value in the corresponding frequency range. These results suggest that the complexity of the simulated signal was the most significant factor for generating the harmonic peaks in the coherence estimation. Our results of the coherence estimation of tremor-related EMGs and STN LFPs obtained from different patients confirmed that (1) harmonic peaks are likely to appear when the tremor-related component is the most dominant one in the STN LFPs; and (2) the non-tremor related component in the STN LFPs may suppress the coherence value selectively depending on its frequency distribution.

We conclude that the harmonic peaks in the coherence estimation of tremor-related neuromuscular signals are related to the degree of distortion in waveform of the tremor-related component and significantly modulated by the non tremor-related component.

Where applicable, the experiments described here conform with Physiological Society ethical requirements.

PC29

DIGITAL DISSECTION AND VISUALISATION OF VIRTUAL TISSUES AND ORGANS USING CONSTRUCTIVE VOLUME GEOMETRY

A.V. Holden[1], M. Chen[2], R.H. Clayton[3], P. Li[1] and J.V. Tucker[2]

[1]Computational Biology Laboratory, School of Biomedical Sciences, University of Leeds, Leeds, UK, [2]Department of Computer Science, University of Wales Swansea, Swansea, UK and [3]Department of Computer Science, University of Sheffield, Sheffield, UK

The computational electromechanics of a contractile organ, such as the beating heart generates both scalar fields (e.g., intra- and extracellular, or transmembrane potentials, and intra- and extracellular ionic activities) and vector fields (e.g., ionic current densities, stresses and strains) within a moving, anisotropic and anatomically sculptured geometry. The dynamics of fluid enclosed by the organ, or vascular perfusion of the tissue itself, can also be obtained. This raises problems of visualisation of a number of different variables and derived quantities (such as action potential duration, or the filament around which re-entrant waves are propagating) within a complicated and moving geometry. Such visualisation may also be coupled with experimental or clinical data streams, and used for computational steering. Traditional scientific visualisation relies on surface representations, that are obtained by transforming field-based data sets.

Volume graphics based on constructive volume geometry (CVG) uses field-based data sets as its intrinsic primitives, and is suited for depicting multiple structures, combinations of different data sets with heterogeneous interior structures by using opacity and combinational operators. CVG has been applied to virtual cardiac tissues (Chen *et al.*, 2003a, b) and is applied to visualise the interior fibre structure that generates anisotropic propagation, to digitally dissect out fibre bundles, and to illustrate propagation in terms of scalar wavefront and vector current densities within a structured anisotropic three-dimensional geometry.

Chen, M. *et al.* (2003a) *Int. J. Bifurcation & Chaos*, **13**, 3591-3604.

Chen, M. *et al.* (2003b) In: Magnin, I.F. *et al.* (Eds.) Functional Imaging and Modeling of the Heart. Lecture Notes in Computer Science 2674, pp30-38. Springer:Berlin.

Supported by EPSRC (GR/R25286 and GR/S43498)

Where applicable, the experiments described here conform with Physiological Society ethical requirements.

PC30

A NEWLY PROPOSED MULTI-SCALE MODEL OF CIRCULATION FOR THE ANALYSIS OF HEART MECHANICS: FROM CELLS TO SYSTEM

E. Shim[1], C. Leem[2] and A. Noma[3]

[1]Department of Mechanical & Biomedical Engineering, Kangwon National Univeristy, Chuncheon, South Korea, [2]Department of Physiology, University of Ulsan, Seoul, South Korea and [3]Department of Physiology, Kyoto University, Kyoto, Japan

A new simulation model coupling single cardiac myocyte mechanics with cardiovascular system is proposed to compute cardiovascular haemodynamics. Electrophysiology of a cardiac cell is numerically approximated by the previous model of human ventricular myocyte. Negroni and Lascano model (NL model) (Negroni & Lascano, 1996) is employed to compute the tension of single cardiac myocyte closely related to ion dynamics in cytoplasm. To convert the tension of single cell to the contractile force of ventricle, we assumed the shape of ventricle as a thin-walled hemispheric shape. A lumped parameter model with seven compartments (Heldt et al. 2002) is utilized to compute systemic circulation interacting with single cardiac cell mechanics via NL model and Laplace law. Numerical simulation shows that the typical characteristics of heart mechanics, such as pressure volume relation, stroke volume and ejection fraction, are successfully reproduced by the proposed multi-scale cardiovascular model covering from single cardiac cell to circulation system. This approach shows that the model of single cardiac myocyte can be integrated to the cardiovascular system by simple approximation.

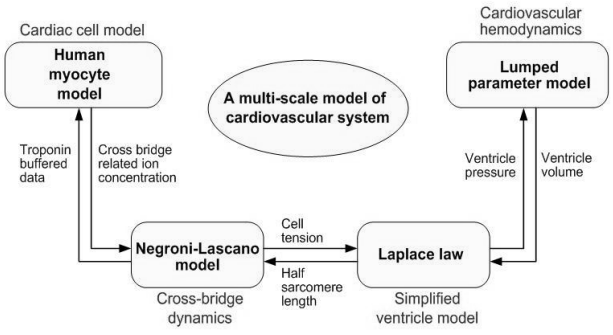

Schematic diagram of a multi-scale model of circulation

Negroni JA & Lascano EC (1996). A cardiac muscle model relating sarcomere dynamics to calcium kinetics. J Mol Cell Cardiol. 28, 915-929.

Heldt T, Shim EB, Kamm RD & Mark RG (2002). J Appl Physiol 92, 1239-1254.

Where applicable, the experiments described here conform with Physiological Society ethical requirements.

PC31

A NEW FRAMEWORK FOR THE INTEGRATION OF MODELS IN BIOLOGY

R. Wright, M. Varela Rey, O. Margoninski, P. Saffrey, J. Hetherington, L. Li, R. Seymour, A. Warner and A. Finkelstein

CoMPLEX, University College London, London, UK

The goal of Systems Biology is to understand large-scale biological systems. The problem often is tackled by building and composing models of biological processes at many different spatio-temporal scales, such as the behaviour of a complete organ derived from the molecular behaviour inside cells. This presents two challenges: integration of heterogeneous biological models and curation of models with the experimental data used to validate them. We aim to develop a robust and scalable approach for model construction and integration, which enables heterogeneous model integration, while allowing a wide variety of models to be executed using the most convenient software tool. The work is part of a DTI-funded Beacon Project to construct an in-silico liver (pizza.cs.ucl.ac.uk/grid/biobeacon), an organ of great medical importance with a relatively homogeneous structure and a dominant cell type, the hepatocyte.

We model elements involved in biological model construction and validation to create a biological meta-model (Atkinson & Kuhne, 2003, Finkelstein et al, 2004). This relates the model, the modelling scheme, embedded assumptions and parameter values or experimental results used to 'run' or interpret the model. It includes results or interpretations obtained from the model, and the software environment.

We use the meta-model to develop a new computational framework consisting of component middleware (Foster et al, 2002) and supporting services for integrating existing, heterogeneous, models. The middleware includes wrappers for software modelling tools, that supply a set of standard interfaces; smart connectors for building composite models; and a coordinator, or workflow execution service, that allows the models to be invoked appropriately. Connectors can, for example, solve numerically a composite model, in which some sub-models form a feedback loop. Thus far we have Mathematica and Xppaut wrappers for ODE based models. Our middleware supports the instantiation of model components using existing modelling tools, and enables communication between components, repositories of experimental data and existing interpretations. The framework supports the execution of composite models built from several sub-models.

Parameters for models are obtained from a repository. Each parameter used in our models is documented according to a detailed schema, with particular attention to linking the parameter information to its experimental basis. The extensible markup language XML is used so that we are able to take advantage of existing tool support, allowing us to browse and present the information in an efficient and accessible manner. We can also perform queries on the data, allowing us to find parameters, for example, based on the work of a particular author, or referring to a specific biological entity. Eventually, this parameter database will form part of a context service that will allow models to automatically gain access to whatever parameter information is appropriate to a specific modelling application.

The results, or interpretations of the models, are stored by the interpretation service. A model repository is used to store existing models, and can be systematically searched to find desired sub-models for creation of new composite models.

We will demonstrate the application of our middleware and wrappers with the computational integration of two models, one written in Xppaut, the other in Mathematica. We shall integrate a model of G-protein coupled receptor signalling with a model of calcium signalling pathways in hepatocytes, using parameters taken from Kummer (2002). We will also show fur-

ther novel strategies for building large integrated models, illustrated by a linked model of the signalling and metabolic pathways associated with glycogenolysis in hepatocytes. Some experimental data to amplify the models will be included.

Atkinson C & Kuhne T (2003). IEEE Software 20, 36-41

Finkelstein A. et al (2004). IEEE Computer 37, 26-33

Foster I. et al (2002). Globus project http://www.globus.org/research/papers

Kummer U et al (2000). Biophysical Journal 79, 1188-1195

Where applicable, the experiments described here conform with Physiological Society ethical requirements.